6. J. Wahr *et al.*, *J. Geophys. Res.* **117**, 1795–1806 (2013).
7. M. Bevis *et al.*, *Geophys. Res. Lett.* **32**, L16308 (2005).
8. P. Bettinelli *et al.*, *Earth Planet. Sci. Lett.* **266**, 332–344 (2008).
9. R. B. Cleveland, W. S. Cleveland, J. E. McRae, I. Terpenning, *J. Off. Stat.* **6**, 3–73 (1990).
10. M. S. Steckler *et al.*, *J. Geophys. Res.* **115**, B08407 (2010).
11. D. Argus, Y. Fu, F. Landerer, *Geophys. Res. Lett.* **41**, 1971–1980 (2014).
12. Materials and methods are available as supplementary materials on *Science* Online.
13. R. A. Bennett, *Geophys. J. Int.* **174**, 1052–1064 (2008).
14. J. L. Davis, B. P. Wernicke, M. E. Tamisiea, *J. Geophys. Res.* **117**, B01403 (2012).
15. D. Dzurisin, *Volcano Deformation: Geodetic Monitoring Techniques* (Springer, New York, 2007).
16. N. E. King *et al.*, *J. Geophys. Res.* **112**, B03409 (2007).
17. D. L. Galloway, T. J. Burbey, *Hydrogeol. J.* **19**, 1459–1486 (2011).
18. P. Elósegui *et al.*, *J. Geophys. Res.* **100**, 9921–9934 (1995).
19. M. A. King *et al.*, *Surv. Geophys.* **31**, 465–507 (2010).
20. K.-H. Ji, T. A. Herring, A. L. Llenos, *Geophys. Res. Lett.* **40**, 1054–1058 (2013).
21. M. E. Ikehara, *Hydrol. Sci. J.* **39**, 417–429 (1994).
22. R. T. Hanson *et al.*, in *Land Subsidence, Associated Hazards, and the Role of Natural Resources Development* (International Association of Hydrological Sciences Press, Wallingford, UK, 2010), vol. 339, pp. 467–471.
23. R. Grapenthin, B. G. Ofeigsson, F. Sigmundsson, E. Sturkell, A. Hooper, *Geophys. Res. Lett.* **37**, L20310 (2010).
24. D. C. Agnew, in *Treatise on Geophysics: Geodesy*, T. A. Herring, Ed. (Elsevier, New York, 2007), pp. 163–195.
25. D. C. Agnew, "SPOTL: Some Programs for Ocean-Tide Loading" (SIO Technical Report, Scripps Institution of Oceanography, La Jolla, CA, 2012); http://escholarship.org/uc/item/954322pg.
26. F. Pollitz, R. Bürgmann, W. Thatcher, *Geochem. Geophys. Geosyst.* **13**, Q06002 (2012).
27. C. B. Amos *et al.*, *Nature* **509**, 483–486 (2014).
28. L. Astiz, P. M. Shearer, D. C. Agnew, *J. Geophys. Res.* **105**, 2937–2953 (2000).
29. B. Smith-Konter, D. Sandwell, P. M. Shearer, *J. Geophys. Res.* **116**, B06401 (2011).
30. M. Van Camp, O. de Viron, L. Métivier, B. Meurers, O. Francis, *Geophys. J. Int.* **197**, 192–201 (2014).
31. G. Ramillien, J. S. Famiglietti, J. Wahr, *Surv. Geophys.* **29**, 361–374 (2008).
32. K. M. Larson *et al.*, *IEEE J. Select. Top. Appl. Earth Obs. Remote Sens.* **3**, 91–99 (2010).
33. E. D. Gutmann, K. M. Larson, M. W. Williams, F. G. Nievinski, V. Zavorotny, *Hydrol. Processes* **26**, 2951–2961 (2012).
34. W. Wan, K. M. Larson, E. E. Small, C. C. Chew, J. J. Braun, *GPS Solut.* 10.1007/s10291-014-0383-7 (2014).
35. J. O. Langbein, F. Wyatt, H. Johnson, D. Hamann, P. Zimmer, *Geophys. Res. Lett.* **22**, 3533–3536 (1995).

ACKNOWLEDGMENTS

The GPS data we use come primarily from the PBO and are publicly available from UNAVCO through the Geodesy Advancing Geosciences and EarthScope Facility, which is supported by the NSF and NASA under NSF cooperative agreement no. EAR-1261833. Meteorological data are publicly available from the National Climatic Data Center's Global Historical Climatology Network. The software used for load computation (SPOTL) is publicly available, and the processing software may be obtained from us. We acknowledge the efforts of many at UNAVCO to produce the exceptional PBO GPS data set, especially the station installation efforts of C. Walls, K. Austin, and K. Feaux. We thank M. Dettinger for comments. This work was supported by USGS grant no. G13AP00059.

SUPPLEMENTARY MATERIALS

www.sciencemag.org/content/345/6204/1587/suppl/DC1
Materials and Methods
Figs. S1 to S9
References

20 June 2014; accepted 8 August 2014
Published online 21 August 2014;
10.1126/science.1260279

EARLY SOLAR SYSTEM

The ancient heritage of water ice in the solar system

L. Ilsedore Cleeves,[1]* Edwin A. Bergin,[1] Conel M. O'D. Alexander,[2] Fujun Du,[1] Dawn Graninger,[3] Karin I. Öberg,[3] Tim J. Harries[4]

Identifying the source of Earth's water is central to understanding the origins of life-fostering environments and to assessing the prevalence of such environments in space. Water throughout the solar system exhibits deuterium-to-hydrogen enrichments, a fossil relic of low-temperature, ion-derived chemistry within either (i) the parent molecular cloud or (ii) the solar nebula protoplanetary disk. Using a comprehensive treatment of disk ionization, we find that ion-driven deuterium pathways are inefficient, which curtails the disk's deuterated water formation and its viability as the sole source for the solar system's water. This finding implies that, if the solar system's formation was typical, abundant interstellar ices are available to all nascent planetary systems.

Water is ubiquitous across the solar system, in cometary ices, terrestrial oceans, the icy moons of the giant planets, and the shadowed basins of Mercury (*1*, *2*). Water has left its mark in hydrated minerals in meteorites, in lunar basalts (*3*), and in martian melt inclusions (*4*). The presence of liquid water facilitated the emergence of life on Earth; thus, understanding the origin(s) of water throughout the solar system is a key goal of astrobiology. Comets and asteroids (traced by meteorites) remain the most primitive objects, providing a natural "time capsule" of the conditions present during the epoch of planet formation. Their compositions reflect those of the gas, dust, and—most important—ices encircling the Sun at its birth, i.e., the solar nebula protoplanetary disk. There remain open questions, however, as to when and where these ices formed, whether they (i) originated in the dense interstellar medium (ISM) in the cold molecular cloud core before the Sun's formation or (ii) are products of reprocessing within the solar nebula (*5*–*7*). Scenario (i) would imply that abundant interstellar ices, including water and presolar organic material, are incorporated into all planet-forming disks. By contrast, local formation within the solar nebula in scenario (ii) would potentially result in large water abundance variations from stellar system to system, dependent on the properties of the star and disk.

In this work, we aim to constrain the formation environment of the solar system's water, using deuterium fractionation as our chemical tracer. Water is enriched in deuterium relative to hydrogen (D/H) compared with the initial bulk solar composition across a wide range of solar system bodies, including comets, (*8*, *9*), terrestrial and ancient martian water (*4*), and hydrated minerals in meteorites (*10*). The amount of deuterium relative to hydrogen of a molecule depends on its formation environment; thus, the D/H fraction in water, $[D/H]_{H_2O}$, can be used to differentiate between the proposed source environments. Interstellar ices, as revealed by sublimation in close proximity to forming young stars, also exhibit high degrees of deuterium enrichment, ~2 to 30 times that of terrestrial water (*11*–*14*). It is not known to what extent these extremely deuterated interstellar ices are incorporated into planetesimals or if, instead, the interstellar chemical record is erased by reprocessing during the formation of the disk (*15*, *16*). Owing to water's high binding energy to grain surfaces, theoretical models predict that water is delivered from the dense molecular cloud to the disk primarily as ice, with some fraction sublimated at the accretion shock in the inner tens of astronomical units (AU) (*15*). If a substantial fraction of the interstellar water is thermally reprocessed, the interstellar deuterated record could then be erased. In this instance, the disk is left as primary source for (re-)creating the deuterium-enriched water present throughout our solar system.

The key ingredients necessary to form water with high D/H are cold temperatures, oxygen, and a molecular hydrogen (H_2) ionization source. The two primary chemical pathways for making deuterated water are (i) gas-phase ion-neutral reactions, primarily through H_2D^+ and (ii) grain-surface formation (ices) from ionization-generated hydrogen and deuterium atoms from H_2. Both reaction pathways depend critically on the formation of H_2D^+. In particular, the gas-phase channel (i) involves the reaction of H_2D^+ ions with atomic oxygen or OH through a sequence of steps to form H_2DO^+, which recombines to form a water molecule. The grain-surface channel (ii) is powered by H_2D^+ recombination with electrons or grains, which liberates hydrogen and deuterium atoms that react with oxygen atoms on cold dust grains. H_2D^+ becomes enriched relative to H_3^+ because the deuterated isotopologue is energetically favored at low temperatures. There is

[1]Department of Astronomy, University of Michigan, 311 West Hall, 1085 South University Avenue, Ann Arbor, MI 48109, USA. [2]Department of Terrestrial Magnetism, Carnegie Institution of Washington, Washington, DC 20015, USA. [3]Harvard-Smithsonian Center for Astrophysics, Harvard University, Cambridge, MA 02138, USA. [4]Department of Physics and Astronomy, University of Exeter, Stocker Road, Exeter EX4 4QL, UK.
*Corresponding author. E-mail: cleeves@umich.edu.

an energy barrier ΔE_1 to return to H_3^+, i.e., $H_3^+ + HD \rightleftharpoons H_2D^+ + H_2 + \Delta E_1$, where $\Delta E_1 \approx 124$ K, although the precise value depends on the nuclear spin of the reactants and products (*17*). The relatively modest value of ΔE_1 restricts deuterium enrichments in H_3^+ to the coldest gas, $T \lesssim 50K$. Thus, deuterium-enriched water formation requires the right mix of environmental conditions: cold gas, gas-phase oxygen, and ionization.

The conditions in the dense interstellar medium, i.e., the cloud core, readily satisfy these requirements, where temperatures are typically $T \approx 10$ K and ionization is provided via galactic cosmic rays (GCRs). In this regard, the conditions in the core and in the outermost regions of the solar nebula are often thought of as analogous (*18*). This is because the outskirts of protoplanetary disks typically contain the coldest ($T \lesssim 30K$), lowest-density gas and are often assumed to be fully permeated by GCRs. However, the efficacy of GCRs as ionizing sources in protoplanetary disks has been called into question because of the deflection of GCRs by the stellar winds produced by young stars (*19*). Even in the mild, modern-day solar wind, the GCR ionization rate, ζ_{GCR}, by a factor of ~100, is below that of the unshielded ISM. Limits on protoplanetary disks' molecular ion emission indicate low GCR ionization rates, $\zeta_{GCR} \leq 3 \times 10^{-17}$ s^{-1} (*20*). In the absence of GCRs, disk midplane ionization is instead provided by scattered x-ray photons from the central star and the decay of short-lived radionuclides (SLRs), where the latter's influence decreases with time (*21*). In addition, the core-disk analogy breaks down with regard to gas density. At the outermost radius of the protosolar gaseous disk, $R_{out} \sim 50$ to 80 AU (*17*), the typical disk density is $n \sim 10^{10}$ cm^{-3}. This value is approximately five orders of magnitude higher than typical values within the interstellar molecular core (*22*). The steady-state ion abundance is proportional to $\sqrt{\zeta/n}$, where ζ is the ionization rate and n is the volumetric gas (hydrogen) density. For a constant ionization rate, a density increase of 10^5 coincides with a factor of ~300 drop in the ion abundance. Thus, wind or magnetically driven deflection of ionizing GCRs, coupled with high gas densities, will strongly inhibit the disk from generating deuterium enrichments through the standard cold chemical reactions (i) and (ii), described above.

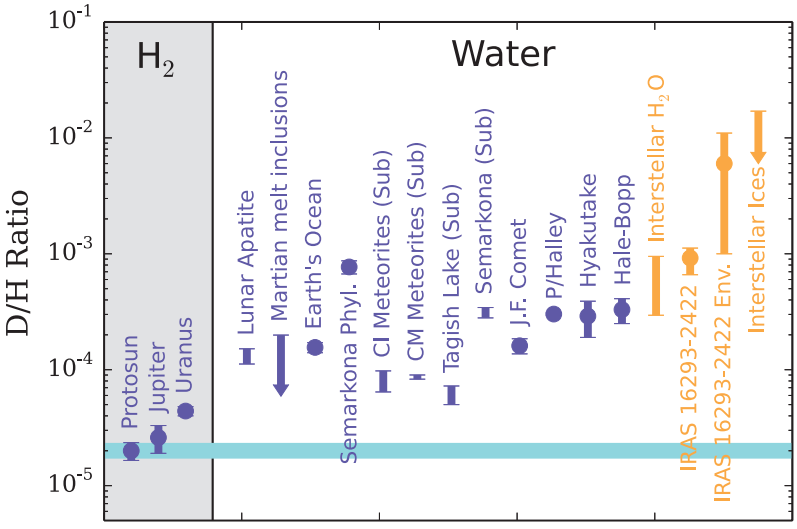

Fig. 1. Atomic D/H ratios in solar system (purple) and interstellar (yellow) sources separated into bulk H_2 and water. Points indicate single measurements, bars without points are ranges over multiple measurements, and arrows correspond to limits. D/H in the bulk gas (i.e., solar) is indicated as a horizontal blue bar. References are provided in table S4 (*17*).

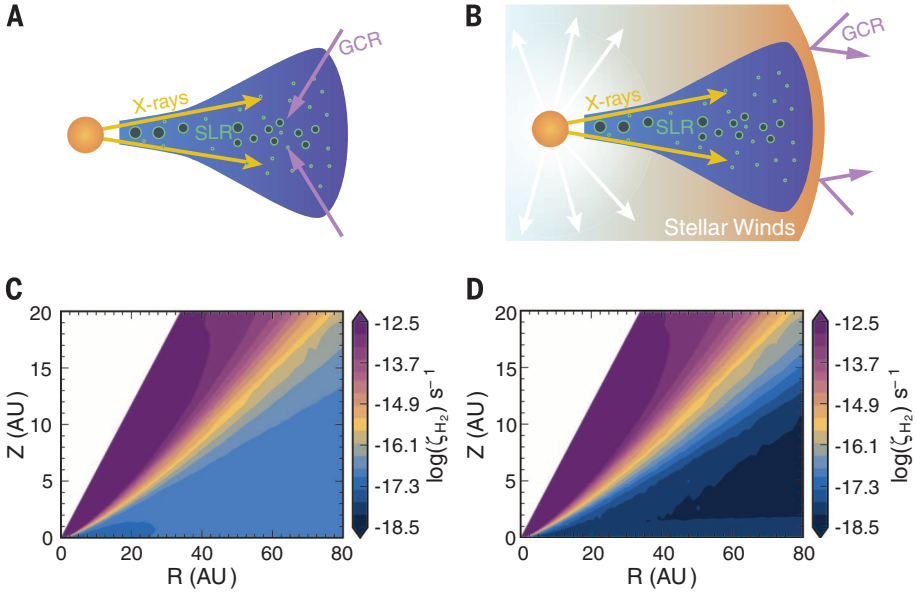

Fig. 2. Schematic of energetic disk ionization sources (top row) and the calculated total H_2 ionization rate (bottom row). (**A**) A "standard" disk ionization model driven by x-rays and GCRs; (**B**) ionization conditions under the influence of a Sun-like wind at solar maximum, now dominated by x-rays in the surface and SLRs in the midplane; (**C**) calculated H_2 ionization rates for the scenario depicted in (A); and (**D**) calculated H_2 ionization rates from the scenario depicted in (B) and that used within this report.

To test the disk hypothesis, we explore whether ionization-driven chemistry within the disk alone is capable of producing the deuterium-enriched water that was present in the early solar system. We have constructed a comprehensive model of disk ionization, including detailed radiative transfer, reduced GCR ionization, and SLR decay. To simulate the "reset" scenario, i.e., all interstellar deuterium enhancement is initially lost, we start with unenriched water with bulk solar D/H composition, $[D/H]_{H_2} = 2.0 \pm 0.35 \times 10^{-5}$ (*23*), and quantify the maximum amount of deuterated water produced by chemical processes in a static protoplanetary disk over 1 million years of evolution. The goal is to determine whether or not the conditions present in the solar nebula were capable of producing at minimum the measured isotopically enriched water in meteorites, ocean water [Vienna Standard Mean Ocean Water (VSMOW)], and comets (see Fig. 1). We do not attempt to address the eventual fate of this water by additional processing, i.e., by radial or vertical mixing, which tends to reduce the bulk D/H ratio in water (*24*, *25*).

Instead, our emphasis is on the physical mechanism necessary for D/H enrichment: ionization. We illustrate the suite of ionization processes considered in the traditional picture of disk ionization (Fig. 2A) alongside a schematic for our new model (Fig. 2B). More specifically, we include "solar-maximum" levels of GCR wind modulation for the incident GCR rate, a factor of ~300 below that of the ISM, Monte Carlo propagation of x-ray photoabsorption and scattering, and ionization by SLR decay products, including losses in the low-density ($\Sigma_{gas} \lesssim 10$ g cm^{-2}) regions of the disk (*17*). The total H_2 ionization rate is shown in Fig. 2, C and D. It can be seen that, whereas the warm surface layers ($\Sigma_{gas} \lesssim 1$ g cm^{-2}) are strongly ionized by stellar x-rays, $\zeta_{XR} \gtrsim 10^{-15}$ s^{-1}, the midplane is comparatively devoid of ionization because of the modulation of incident GCRs (Fig. 2D).

To compute molecular abundances, we compile a simplified deuterium-reaction network designed to robustly predict the D/H in water resulting from gas-phase and grain-surface chemistry (*17*). We include both ion-neutral and the hot-phase neutral-neutral water chemistry (*26*), as well as self-shielding by HD and D_2, in addition to the standard chemical network (*17*). We include an updated treatment of the inherently surface-dependent CO freeze-out process, motivated by new laboratory data on CO ice-binding energies (*17*). CO freeze-out is important for the present study, as CO regulates the amount of oxygen present in gas above $T > 17$ K and available for new water formation. We place the majority of volatile carbon in CO and the rest of the oxygen not in CO in water ice (*15*) [see supplementary materials for additional runs (*17*)]. We examine the final D/H of water ice after 1 million years of chemical evolution, i.e., the approximate lifetime of the gas-rich disk and, correspondingly, the duration over which the disk is able to build up deuterated water (see Fig. 3). The ions are most abundant in the upper, x-ray–dominated surface layers, whose temperatures are too warm for substantial deuterium enrichment in $[D/H]_{H_3^+}$. The bulk ice mass is closest to the cold midplane, where only a meager amount (per unit volume) of H_3^+ and H_2D^+ remain in the gas, a consequence of low ionization rates and high densities.

In addition to spatial abundances, we provide ratios of the vertically integrated column densities of both ions and ices (Fig. 3, bottom). The choice of VSMOW as a benchmark is somewhat arbitrary, considering that comets exceed D/H in VSMOW by factors of one to three times and meteorites have typically lower values, a factor ~2 less (Fig. 1). The column-derived $[D/H]_{H_3^+}$ approaches—but does not reach—VSMOW after 1 million years at the outer edge of the disk. Moreover, most of the molecules that contribute to the column density ratio of $[D/H]_{H_3^+}$ arise in an intermediate layer of cold (T_{gas} ~ 30 to 40 K) gas, where x-ray photons are still present. However, it is readily apparent that this enrichment does not translate into $[D/H]_{H_2O}$. The most deuterium-enriched water, $[D/H]_{H_2O} = 3 \times 10^{-5}$, is colocated with the enriched layer of $[D/H]_{H_3^+}$; however, the water is considerably less enriched than the ions. Over the lifetime of the disk, the gas-phase and grain-surface chemical pathways do not produce deuterated water ices in substantial quantities. Water production is low because of a combination of (i) a lack of sufficient ionization to maintain large amounts of H_2D^+ in the gas and (ii) a lack of atomic oxygen in the gas, locked up in ices. We do find a superdeuterated layer of water at the disk surface ($[D/H]_{H_2O} = 5 \times 10^{-3}$). This layer is a direct consequence of selective self-shielding of HD relative to H_2, which leads to an overabundance of atomic D relative to H. Selective self-shielding is also the cause of the fall of $[D/H]_{H_3^+}$ below the initial bulk gas value inside of $R < 40$ AU. This layer does not, however, contribute substantially to the vertically integrated $[D/H]_{H_2O}$ (Fig. 3, bottom).

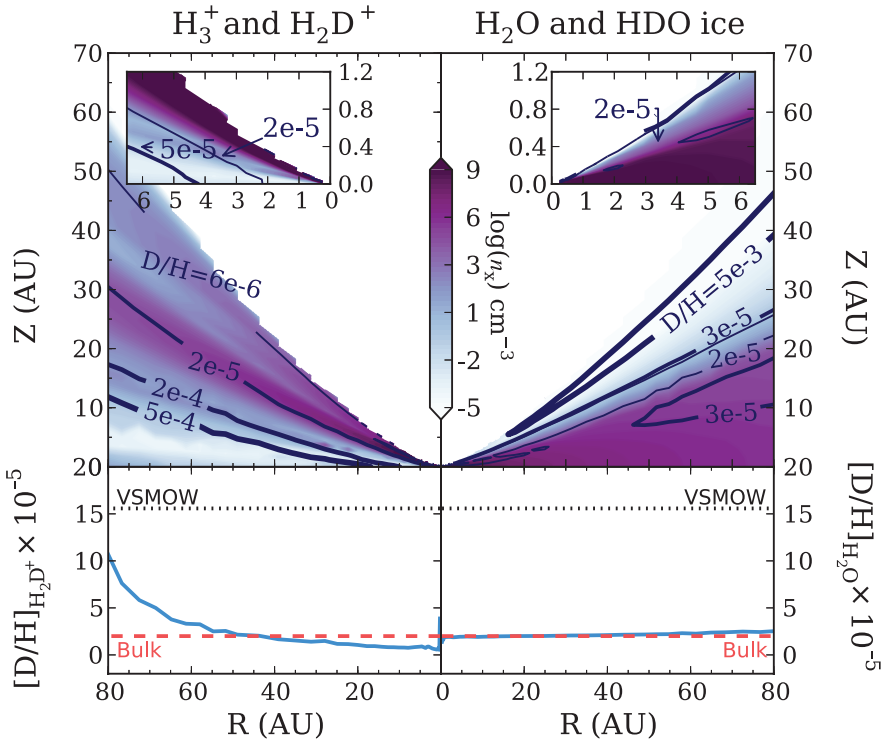

Fig. 3. Chemical abundances and column densities for the drivers of the deuterium enrichment, the ions; and the corresponding products, the ices. (**Top**) Volume densities (cm^{-3}) of all labeled isotopologues for H_3^+ (left) and water (right) in filled purple contours. Solid contour lines indicate local D/H and are as labeled. The color scale applies to both the left and right halves of the plot. (**Insets**) Enlarged inner disk with the same axis units. (**Bottom**) Plots of the vertically integrated D/H ratio of column densities versus radius. The bulk gas (protosolar) value is labeled by the red dashed line, and Earth's ocean value (VSMOW) is labeled with the black dotted line.

In summary, using a detailed physical ionization model, updated treatment of oxygen-bearing (CO) ice chemistry, and a simplified deuterium chemical network, we find that chemical processes in disks are not efficient at producing noteworthy levels of highly deuterated water. Our model predicts that disk chemistry can only produce a volume-integrated $[D/H]_{H_2O} \lesssim 2.1 \times 10^{-5}$, which is only slightly enriched from the bulk solar value (2×10^{-5}). In terms of column density, we find that, even in the most radially distant (coldest) regions, water only attains $[D/H]_{H_2O} \lesssim 2.5 \times 10^{-5}$. This finding implies that ion chemistry within the disk cannot create the deuterium-enriched water present during the epoch of planet formation. When we begin our models with interstellar $[D/H]_{H_2O} \sim 10^{-3}$, however, it is hard to "erase" D/H ratios with low-temperature disk chemistry alone. A number of studies have invoked turbulent mixing of gas in the radial and/or vertical directions, which can reduce inner-disk deuterium enrichments in water (*24*, *25*, *27*). Moreover, a common feature of such models is that they begin with high levels of deuterated water, as high as $[D/H]_{H_2O} \sim 10^{-2}$. In general, mixing in the vertical direction transports highly deuterium–enriched ices from the shielded midplane into the x-ray– and ultraviolet-irradiated warm surface layers (*28*, *29*), where they can be reprocessed to lower D/H. Ices transported radially inward, either entrained by gas accretion or subjected to radial migration, evaporate in the warm and dense inner disk and isotopically reequilibrate with H_2 or ion-neutral chemistry in hot ($T > 100$ K) gas. With our updated disk ionization model, we can now exclude chemical processes within the disk as an enrichment source term and conclude that the solar nebula accreted and retained some amount of pristine interstellar ices. One potential explanation is that during the formation of the disk, there was an early high-temperature episode followed by continued infall from deuterium-enriched interstellar ices (*16*). If we ignore the negligible contribution to deuterated water formation from the disk, we can estimate the fraction of water in a particular solar system body, X, that is presolar, $f_{ISM} = (D/H_X - D/H_\odot)/(D/H_{ISM} - D/H_\odot)$, where D/H_X refers to $[D/H]_{H_2O}$ in X and $D/H_\odot = 2 \times 10^{-5}$. Water in the ISM ranges from a limit of $[D/H]_{H_2O} < 2 \times 10^{-3}$ in interstellar ice (*11*) to $[D/H]_{H_2O} = (3 \text{ to } 5) \times 10^{-4}$ for low-mass protostars, i.e., analogs to the Sun's formation environment (*14*). If the former, higher value reflects the ices accreted by the solar nebular disk, then, at the very least, terrestrial oceans and comets should contain ≳7% and ≳14% interstellar water, respectively. If the low-mass protostellar values are representative, the numbers become 30 to 50% for terrestrial oceans and 60 to 100% for comets. Thus, a considerable fraction of the solar system's water predates the Sun. These findings imply that some amount of interstellar ice survived

the formation of the solar system and was incorporated into planetesimal bodies. Consequently, if the formation of the solar nebula was typical, our work implies that interstellar ices from the parent molecular cloud core—including the most fundamental life-fostering ingredient, water—are widely available to all young planetary systems.

REFERENCES AND NOTES

1. T. Encrenaz, *Annu. Rev. Astron. Astrophys.* **46**, 57–87 (2008).
2. D. J. Lawrence *et al.*, *Science* **339**, 292–296 (2013).
3. J. J. Barnes *et al.*, *Earth Planet. Sci. Lett.* **390**, 244–252 (2014).
4. T. Usui, C. M. O'D. Alexander, J. Wang, J. I. Simon, J. H. Jones, *Earth Planet. Sci. Lett.* **357-358**, 119–129 (2012).
5. F. Robert, D. Gautier, B. Dubrulle, *Space Sci. Rev.* **92**, 201–224 (2000).
6. C. Ceccarelli *et al.*, in *Protostars and Planets VI*, H. Beuther *et al.*, Eds. (Univ. of Arizona, Tucson, 2014), pp. 859–882.
7. E. F. van Dishoeck, E. A. Bergin, D. C. Lis, J. I. Lunine, in *Protostars and Planets VI*, H. Beuther *et al.*, Eds. (Univ. of Arizona, Tucson, 2014), pp. 835–858.
8. D. Bockelée-Morvan *et al.*, *Icarus* **133**, 147–162 (1998).
9. P. Eberhardt, M. Reber, D. Krankowsky, R. R. Hodges, *Astron. Astrophys.* **302**, 301 (1995).
10. C. M. O'D. Alexander *et al.*, *Science* **337**, 721–723 (2012).
11. E. Dartois *et al.*, *Astron. Astrophys.* **399**, 1009–1020 (2003).
12. A. Coutens *et al.*, *Astron. Astrophys.* **539**, A132 (2012).
13. M. V. Persson, J. K. Jørgensen, E. F. van Dishoeck, *Astron. Astrophys.* **541**, A39 (2012).
14. M. V. Persson, J. K. Jørgensen, E. F. van Dishoeck, D. Harsono, *Astron. Astrophys.* **563**, A74 (2014).
15. R. Visser, E. F. van Dishoeck, S. D. Doty, C. P. Dullemond, *Astron. Astrophys.* **495**, 881–897 (2009).
16. L. Yang, F. J. Ciesla, C. M. O'D. Alexander, *Icarus* **226**, 256–267 (2013).
17. Materials and methods are available as supplementary material on *Science* Online.
18. Y. Aikawa, E. Herbst, *Astrophys. J.* **526**, 314–326 (1999).
19. L. I. Cleeves, F. C. Adams, E. A. Bergin, *Astrophys. J.* **772**, 5 (2013).
20. E. Chapillon, B. Parise, S. Guilloteau, F. Du, *Astron. Astrophys.* **533**, A143 (2011).
21. T. Umebayashi, N. Katsuma, H. Nomura, *Astrophys. J.* **764**, 104 (2013).
22. T. Minamidani *et al.*, *Astron. J.* **141**, 73 (2011).
23. J. Geiss, G. Gloeckler, *Space Sci. Rev.* **106**, 3–18 (2003).
24. K. Willacy, P. M. Woods, *Astrophys. J.* **703**, 479–499 (2009).
25. T. Albertsson, D. Semenov, T. Henning, *Astrophys. J.* **784**, 39 (2014).
26. E. A. Bergin, W. D. Langer, P. F. Goldsmith, *Astrophys. J.* **441**, 222 (1995).
27. K. Furuya, Y. Aikawa, H. Nomura, F. Hersant, V. Wakelam, *Astrophys. J.* **779**, 11 (2013).
28. F. J. Ciesla, S. A. Sandford, *Science* **336**, 452–454 (2012).
29. F. J. Ciesla, *Astrophys. J.* **784**, L1 (2014).

ACKNOWLEDGMENTS

L.I.C. and E.A.B. acknowledge support by NSF grant AST-1008800. C.M.O'D.A. was partially supported by NASA Astrobiology grant NNA09DA81A and by NASA Cosmochemistry grant NNX11AG67G. F.D. was supported by NASA grant NNX12A193G. T.J.H. was supported by U.K. Science and Technology Facilities Council grant ST/J001627/1.

SUPPLEMENTARY MATERIALS

www.sciencemag.org/content/345/6204/1590/suppl/DC1
Materials and Methods
Figs. S1 to S4
Tables S1 to S4
References (*30*–*71*)

30 June 2014; accepted 21 August 2014
10.1126/science.1258066

WATER SPLITTING

Water photolysis at 12.3% efficiency via perovskite photovoltaics and Earth-abundant catalysts

Jingshan Luo,[1,2] Jeong-Hyeok Im,[1,3] Matthew T. Mayer,[1] Marcel Schreier,[1] Mohammad Khaja Nazeeruddin,[1] Nam-Gyu Park,[3] S. David Tilley,[1] Hong Jin Fan,[2] Michael Grätzel[1]*

Although sunlight-driven water splitting is a promising route to sustainable hydrogen fuel production, widespread implementation is hampered by the expense of the necessary photovoltaic and photoelectrochemical apparatus. Here, we describe a highly efficient and low-cost water-splitting cell combining a state-of-the-art solution-processed perovskite tandem solar cell and a bifunctional Earth-abundant catalyst. The catalyst electrode, a NiFe layered double hydroxide, exhibits high activity toward both the oxygen and hydrogen evolution reactions in alkaline electrolyte. The combination of the two yields a water-splitting photocurrent density of around 10 milliamperes per square centimeter, corresponding to a solar-to-hydrogen efficiency of 12.3%. Currently, the perovskite instability limits the cell lifetime.

Compared with other energy resources, solar energy is sustainable and far more abundant than our projected energy needs as a species; thus, it is considered as the most promising energy source for the future. Because of the diffuse nature of solar energy, large arrays of solar cells will have to be implemented. Currently, electricity produced by silicon (Si) solar cells is too costly to achieve grid parity. In contrast, the dye-sensitized solar cell (DSSC) (*1*, *2*) uses cheap materials and facile solution processes. A related type of low-cost solution-processed solar cell based on a perovskite formulation has recently emerged (*3*–*10*). The rapid rise of the solar-to-electric power conversion efficiency (currently 17.9% certified) in less than 5 years makes it highly promising for large-scale commercialization (*11*). Long-term stability, however, is currently a challenge with these solar cells.

The conversion of solar energy directly into fuels is a promising solution to the challenge of intermittency in renewable energy sources, addressing the issues of effective storage and transport. In nature, plants harvest solar energy and convert it into chemical fuel via photosynthesis. Inspired by nature, artificial photosynthesis has been proposed as a viable way to store the solar energy as fuel (*12*, *13*). Hydrogen, which is the simplest form of energy carrier, can be generated renewably with solar energy through photoelectrochemical water splitting or by photovoltaic (PV)–driven electrolysis. Intensive research has been conducted in the past several decades to develop efficient photoelectrodes, catalysts, and device architectures for solar hydrogen generation (*14*–*20*). However, it still remains a great challenge to develop solar water-splitting systems that are both low-cost and efficient enough to generate fuel at a price that is competitive with fossil fuels (*21*).

Splitting water requires an applied voltage of at least 1.23 V to provide the thermodynamic driving

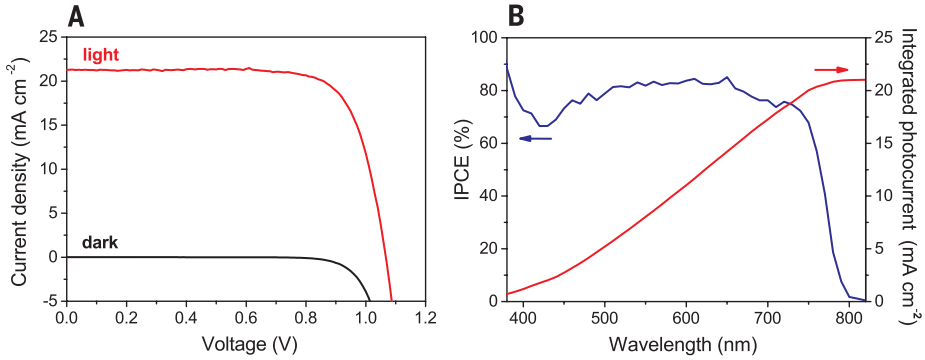

Fig. 1. Performance of perovskite solar cell. (**A**) Current density–potential curve (*J*–*V*) of the perovskite solar cell under dark and simulated AM 1.5G 100 mW cm^{-2} illumination. (**B**) IPCE spectrum of the perovskite solar cell and the integrated photocurrent with the AM 1.5G solar spectrum.

[1]Laboratory of Photonics and Interfaces, Institute of Chemical Sciences and Engineering, School of Basic Sciences, Ecole Polytechnique Fédérale de Lausanne (EPFL), CH-1015 Lausanne, Switzerland. [2]Division of Physics and Applied Physics, School of Physical and Mathematical Sciences, Nanyang Technological University (NTU), 637371 Singapore. [3]School of Chemical Engineering and Department of Energy Science, Sungkyunkwan University (SKKU), Suwon 440-746, Korea.
***Corresponding author. E-mail: michael.graetzel@epfl.ch**

Science
AAAS

The ancient heritage of water ice in the solar system

L. Ilsedore Cleeves *et al.*

Science **345**, 1590 (2014);
DOI: 10.1126/science.1258055